Resonant phonon scattering of paraexcitons in Cu_2O

Christian Sandfort,* Jan Brandt, Dietmar Fröhlich, and Manfred Bayer
Institut für Physik, Technische Universität Dortmund, D-44221 Dortmund, Germany

Heinrich Stolz
Fachbereich Physik, Universität Rostock, D-18501 Rostock, Germany

(Received 28 April 2008; published 1 July 2008)

The paraexciton in Cu_2O is optically forbidden to all orders. By means of a magnetic field, it obtains oscillator strength from the quadrupole allowed orthoexciton. With an external magnetic field, we are able to excite resonantly ultracold paraexcitons. We observe a pronounced resonant Raman signal on top of the luminescence from thermalized paraexcitons. We present the magnetic-field dependence of the Γ_3^- phonon replica of the paraexciton. In addition, we show the spectra of the Γ_2^-, Γ_4^-, and Γ_5^- phonon sidebands. We are even able to observe two-phonon scattering of the paraexciton.

DOI: 10.1103/PhysRevB.78.045201 PACS number(s): 78.20.−e, 78.30.−j, 71.35.Lk

I. INTRODUCTION

Resonant optical-phonon (LO and TO) scattering from orthoexcitons in Cu_2O was extensively studied in the past.[1,2] Recently acoustic- and optical-phonon scattering in high magnetic fields was reported.[3] It was shown that longitudinal-acoustic (LA) as well as transverse-acoustic (TA) phonon scattering has to be considered to analyze the rich spectrum of inter- and intraband processes. LO-phonon-scattering processes are of special interest, since the almost dispersionless optical phonons allow us to study directly the thermal distribution in search of the Bose-Einstein condensation (BEC) of excitons.[4] The paraexciton in Cu_2O is the favored candidate for BEC, since it is the exciton of lowest energy with a long lifetime on the order of a microsecond[5] compared to the orthoexcitons with a lifetime of only a few nanoseconds.[6] From the paraexciton of Γ_2^+ symmetry, only the scattering by a Γ_5^- phonon dipole is allowed. Since the paraexciton is forbidden for direct optical excitation, the Γ_5^- phonon sideband has been detected only by higher-energy excitation (band to band, orthoexciton) and subsequent relaxation by TA-phonon emission to the paraexciton.[7,8] In a magnetic field B, however, the paraexciton gains quadrupole oscillator strength from the orthoexciton.[9,10] The orthoexciton splits into three components ($M=0, \pm 1$). The $M=0$ component of the Γ_5^+ orthoexciton mixes with the Γ_2^+ paraexciton and gives rise to a paraexciton polariton and thus a resonance for one-photon absorption. This resonance was recently measured as a narrow absorption band with a half-width of 80 neV.[11] As a consequence, in addition to the Γ_5^- phonon, other optical phonons of Γ_2^-, Γ_3^-, and Γ_4^- symmetries become allowed. These additional phonon sidebands of the paraexciton can be seen either by excitation in the orthoexciton or by resonant excitation in the paraexciton, thus yielding resonant optical-phonon scattering which, up to now, has been observed only for the orthoexciton. By excitation in the orthoexciton, the intensity of the Γ_3^- phonon sideband shows a perfect B^2 dependence as expected from the field-induced mixing. By direct excitation it is now possible to detect resonant Raman scattering from the paraexciton with the polarization selection rules of the $M=0$ component.[3] In connection with the observation of BEC of paraexcitons, there is hope that LO-phonon scattering from a condensate (macroscopic occupation of excitons at $k=0$) might be distinguishable from resonant Raman scattering from $k=k_0$ (photon wave number). As was shown for the orthoexcitons,[2] there are scattering processes with two optical phonons. We are able to resolve two-phonon sidebands of paraexcitons.

The paper is organized as follows: After a short section on the theory of magnetic field–induced mixing of ortho- and paraexcitons and the polarization selection rules for optical-phonon scattering from paraexcitons, we will describe in Sec. III the experimental setup. In Sec. IV we present our experimental results and a discussion, and in Sec. V we present a conclusion.

II. THEORY

In this section we briefly introduce the theory of field-induced mixing of ortho- and paraexcitons. In a magnetic field B, the degeneracy of the threefold orthoexciton is lifted and it splits into three components $M=0$ and $M=\pm 1$. The interaction can be expressed by the following matrix in the basis of the Γ_2^+ paraexciton and the three orthoexciton states $M=0$, $M=\pm 1$:

$$\hat{H}_B = \begin{pmatrix} -\varepsilon & i\alpha B & 0 & 0 \\ -i\alpha B & 0 & 0 & 0 \\ 0 & 0 & \beta B & 0 \\ 0 & 0 & 0 & -\beta B \end{pmatrix}, \tag{1}$$

with the coefficients $\alpha=92.5$ μeV/T and $\beta=47.7$ μeV/T describing the coupling of the ortho- and paraexciton states and the splitting of the orthoexcitons, respectively.[3]

This interaction matrix [Eq. (1)] shows that the Γ_2^+ paraexciton state mixes only with the $M=0$ component of the orthoexciton. The admixture can be described by the field-induced mixing coefficient[11]

$$a_O = \frac{\alpha B}{\sqrt{(\alpha B)^2 + \varepsilon^2}} \approx \frac{\alpha B}{\varepsilon}. \quad (2)$$

Due to this admixture, the paraexciton gains oscillator strength from the quadrupole allowed orthoexciton,

$$f_P = \left(\frac{\alpha B}{\epsilon}\right)^2 f_O = 5.8 \times 10^{-5} f_O B^2, \quad (3)$$

where f_P is the paraexciton and $f_O = 3.7 \times 10^{-9}$ (Ref. 12) is the oscillator strength of the orthoexciton.

It has been shown that the k^2-dependent exchange interaction[13] leads to a splitting of the threefold degenerate orthoexciton. The perturbation due to this interaction, however, can be neglected since it is only 5 μeV, compared to the splitting $\Delta E_{\pm 1} = 954$ μeV at 10 T. The diagonalization of the matrix [Eq. (1)] yields the new eigenstates $\mathbf{\Psi}(\mathbf{B})$.

For a given polarization $\mathbf{e}$ of the outgoing light, the relative oscillator strength $O\Psi_j$ for optical-phonon emission is given by

$$O\Psi_j = \sum_{i=1}^{g_j} |\mathbf{e}\hat{\sigma}_i^j \mathbf{\Psi}(\mathbf{B})|^2. \quad (4)$$

g_j denotes the degeneracy of the optical phonon j ($j = 2,3,4,5$) and $\hat{\sigma}_i^j$ is the coupling matrix of the phonon. The component of the paraexciton wave function $\mathbf{\Psi}(\mathbf{B})$ with Γ_2^+ symmetry can couple only to a Γ_5^- phonon, whereas the orthoexciton admixture of Γ_5^+ symmetry ($M=0$ component) can couple also to the other phonons (Γ_2^-, Γ_3^-, and Γ_4^-). The polarization selection rules for Γ_3^-, Γ_4^-, and Γ_5^- phonon emission for the orthoexciton ($M=0$ component) are given in Ref. 3. Since the coupling matrix between the Γ_5^+ states ($M=0$ component of the orthoexciton) and the dipole operator (Γ_4^-) via the Γ_2^- phonon is diagonal,[14] the polarization selection rules of the Γ_2^- phonon replica are the same as for the $\Gamma_{5i}^+ (i = x,y,z)$ components of the quadrupole excited $M=0$ state.

As the dispersion of the Γ_2^-, Γ_3^-, and Γ_5^- optical phonons and the longitudinal component of the Γ_4^- phonon can be neglected close to the zone center, the optical-phonon luminescence exhibits directly the thermal distribution of paraexcitons $N_P(E)$. For the transversal components of the dipole allowed Γ_4^- phonon, however, the dispersion (phonon polariton branches) has to be taken into account.

III. EXPERIMENTAL SETUP

The high-resolution setup is shown schematically in Fig. 1. We use a single-frequency dye laser with a bandwidth of about 5 neV (Coherent 899-29) pumped by a solid-state laser (Verdi V-10). The high resolution of the laser allows ultracold resonant excitation of paraexcitons at k_0 with a kinetic energy of 13.2 μeV (0.15 K) for a paraexciton mass of $M_P = 2.61$.[11] About 10% of the laser light is coupled into a diagnostic setup consisting of a 300 MHz scanning Fabry-Pérot spectrum analyzer (SA), a beam profile analyzer, and a wave meter with an absolute accuracy of 30 MHz. With the aid of this diagnostic setup, we ensure stable excitation at $k=k_0$ with a TEM_{00} Gaussian mode. The light beam passes a

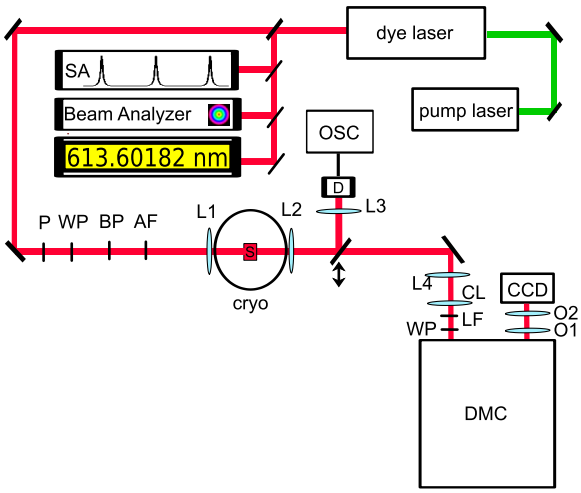

FIG. 1. (Color online) Schematic setup for high-resolution spectroscopy: AF, attenuation filter; BP, bandpass filter; CCD, charge coupled device camera; CL, cylindrical lens; cryo, magneto-optic cryostat; D, diode; DMC, double monochromator; L1, L2, L3, and L4, lenses; LF, low-frequency pass filter; P, polarizer; O1 and O2, objectives; OSC, oscilloscope; S, sample; SA, spectrum analyzer; WP, half-wave plate.

polarizer (P), a half-wave plate (WP) used to choose the appropriate polarization of the $M=0$ component, a bandpass filter (BP) used to suppress amplified spontaneous emission (ASE) from the laser, and an attenuation filter (AF). Suppression of ASE is crucial, since in the spectral region of the phonon-assisted luminescence, the intensity of the observed luminescence is on the same order of magnitude as the intensity of the ASE. The laser beam is focused (L1) onto a spot of 30 μm on the sample (S). The samples are cut from a natural crystal and mounted strain-free in a split coil cryostat. They are immerged in liquid helium inside a variable temperature insert (VTI) and cooled to a temperature of about 1.2 K by pumping on the VTI. The cryostat allows the application of a magnetic field in Faraday ($\mathbf{B} \| \mathbf{k}$) and Voigt configurations ($\mathbf{B} \perp \mathbf{k}$) up to 10 T. The light transmitted through the sample is detected by a diode (D) on a 1.5 GHZ oscilloscope (OSC). The transmission was always monitored prior to the luminescence measurement for two reasons: (i) selection of a strain-free part of the sample with narrow resonance and (ii) tuning into resonance for maximum absorption. For further details on transmission experiments, we refer the reader to Ref. 12. For detection of the luminescence, the transmitted light is collected (L2) and focused (L4) onto the entrance slit of a double monochromator (DMC) with a focal length of 0.85 m. The ratio of the selected focal lengths of L2 and L4 leads to two times enlarged images of the sample on the entrance slit. A cylindrical lens (CL) in front of the monochromator corrects for astigmatism. A half-wave plate (WP) in front of the entrance slit allows the rotation of the polarized luminescence into the preferred polarization plane of the monochromator. A low-frequency pass filter (LF) is used to suppress scattered laser light. Two objectives (O1 and O2) behind the exit slit of the monochromator yield a four times magnified image of the plane of the exit slit on the nitrogen-cooled charge coupled device (CCD) camera

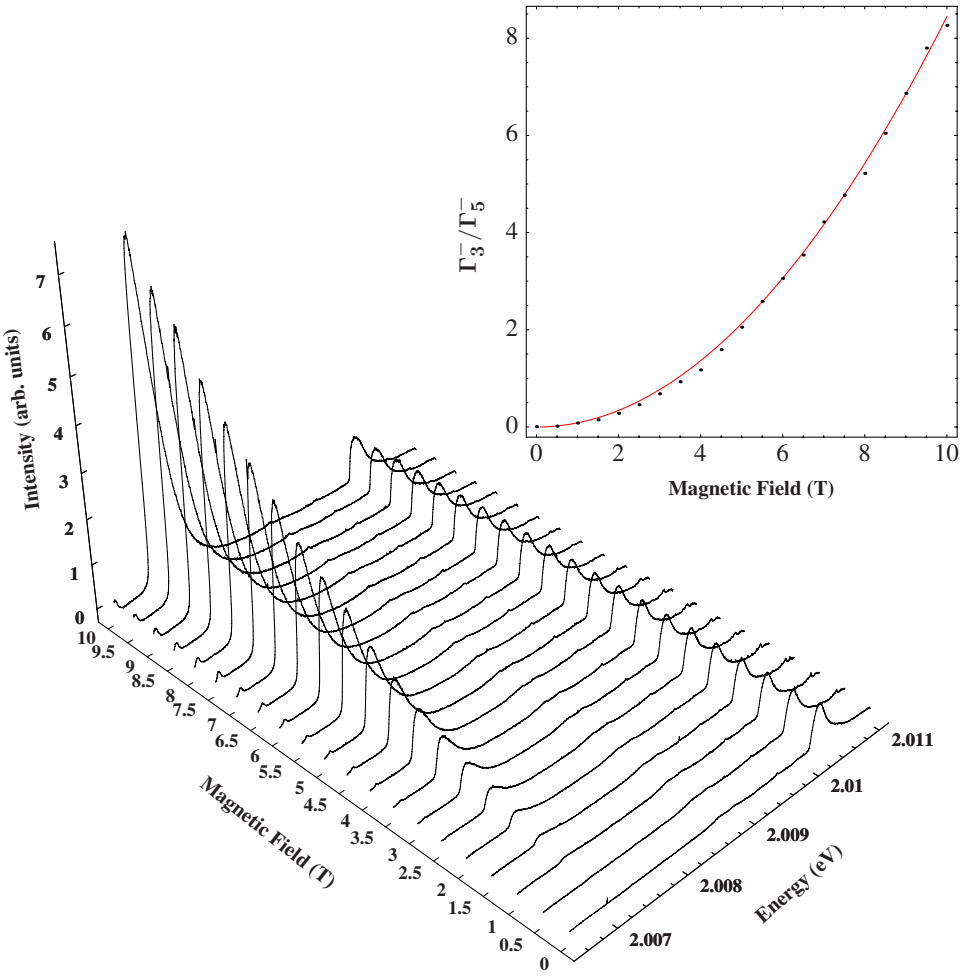

FIG. 2. (Color online) Magnetic-field dependence of the Γ_3^- and Γ_5^- phonon-assisted luminescence of paraexciton at 1.2 K for excitation in the orthoexciton. Inset: ratio Γ_3^-/Γ_5^- of integrated luminescence of phonon replica of Γ_3^- and Γ_5^-; solid line: B^2 dependence.

(pixel size 25 μm). With this setup we achieve in second order a resolution of about 10 μeV.

IV. EXPERIMENTAL RESULTS AND DISCUSSION

In the following we present our experimental results. Without external perturbation, only the Γ_5^- phonon couples with a photon (Γ_4^- dipole) to the paraexciton ($\Gamma_2^+ \otimes \Gamma_5^- = \Gamma_4^-$). The $\Gamma_2^-, \Gamma_3^-, \Gamma_4^-$ phonon emission is forbidden [$\Gamma_2^+ \otimes (\Gamma_2^-, \Gamma_3^-, \Gamma_4^-) \neq \Gamma_4^-$]. In a magnetic field they become allowed by the admixture [coefficient a_O, Eq. (2)] of the $M=0$ component of the Γ_5^+ orthoexciton into the paraexciton [Γ_4^- is contained in $\Gamma_5^+ \otimes (\Gamma_2^-, \Gamma_3^-, \Gamma_4^-)$]. In order to study the B-field dependence of the Γ_3^- phonon emission of the paraexciton, we excite in the orthoexciton resonance ($M=0$ component), since orthoexcitons convert to paraexcitons[7] and the orthoexciton absorption is expected to be independent of the magnetic field. Figure 2 shows spectra of the Γ_3^- and Γ_5^- phonon-assisted luminescence of the paraexciton as a function of magnetic field. The dependence of the ratio of the integrated luminescence intensity of the Γ_3^- and Γ_5^- phonon replica on the magnetic field is plotted in the inset of Fig. 2. The solid line represents the ratio calculated from Eq. (3). The experimental data follow the expected B^2 dependence.

Figure 3 shows the Γ_3^- and Γ_5^- phonon replica of the paraexciton for excitation in the paraexciton resonance at 10 T. Subtracting the thermal distribution from the spectrum yields resonances (Fig. 4), which are interpreted as a resonance Raman effect (ingoing resonance at $k=k_0$). $E=0$ corresponds to $E(0)-E(\Gamma_i^-)$, $i=3,5$, with an uncertainty of $\pm 5\mu$eV, showing that the resonances are not at $k=0$ but at $k=k_0$. The resonances can be fitted by Lorentzians of width γ_i ($i=3,5$) of the corresponding phonon convolved with a slit function to account for the finite spectral resolution of

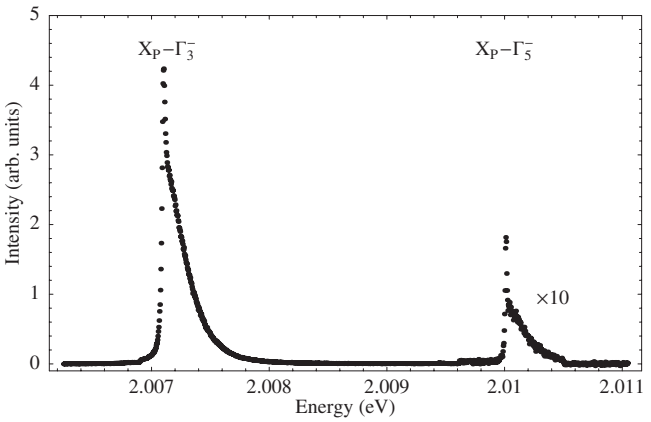

FIG. 3. Γ_3^- and Γ_5^- phonon replica of paraexciton for resonant excitation of paraexciton at 10 T and 1.2 K. Note a factor of 10 enlargement of Γ_5^- replica.

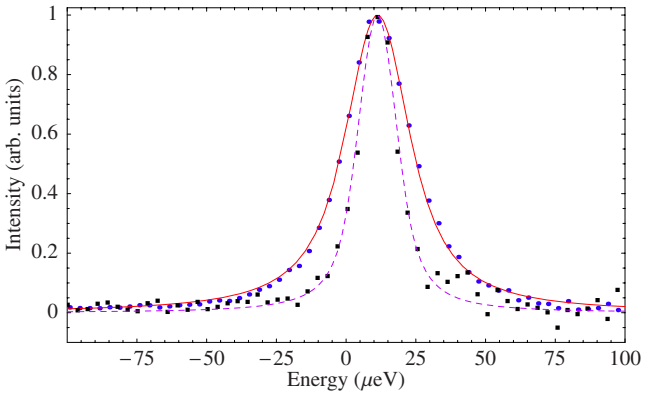

FIG. 4. (Color online) Resonance Raman lines from Fig. 3 after subtraction of thermal distribution. Full line and dots, Γ_3^- phonon; dashed line and squares, Γ_5^- phonon. $E=0$ corresponds to $E(0)-E(\Gamma_i^-)$, $i=3,5$. Solid ($i=3$) and dashed ($i=5$) lines: fits to data by Lorentzians of width γ_i and corrected for finite spectral resolution (10 μeV).

10 μeV. As shown in Fig. 4, the damping $\gamma_3 \approx 25$ μeV of the Γ_3^- phonon is a factor of 2 larger than the damping $\gamma_5 \approx 11$ μeV of the Γ_5^- phonon. As the kinetic energy $E(k_0)$ is 13.2 μeV (Ref. 11) above $E(0)$, the small width of the Γ_5^- peak should allow the identification of an extra peak from a phonon emission from a BEC at $k=0$. Up to now there is no evidence for such a scenario.

Figure 5 shows the intensity dependence of the Γ_3^- Raman peak on laser energy. The solid line shows an absorption spectrum measured on the same sample. There are deviations between the absorption and emission data mainly in the tails, which might be due to the fact that different spots on the sample were used in the absorption and emission experiments. Tuning the energy of the exciting laser shows a linear dependence of the energetic position of the Γ_3^- Raman peak on the laser energy as it is expected for a Raman transition (inset of Fig. 5). Both the intensity dependence of the peak and the linear dependence of the peak energy on laser energy confirm the interpretation of the peak as a resonance Raman effect.

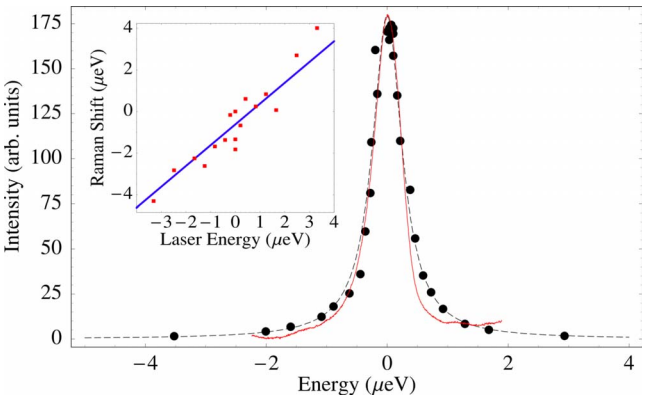

FIG. 5. (Color online) Dependence of Γ_3^- Raman peak on laser energy. Filled dots: experimental results; dashed line: fit to data by a Lorentzian; full line: absorption spectrum measured on the same sample. Inset: dependence of the Γ_3^- Raman peak on laser energy; solid line: fit to data by a line with slope 1.

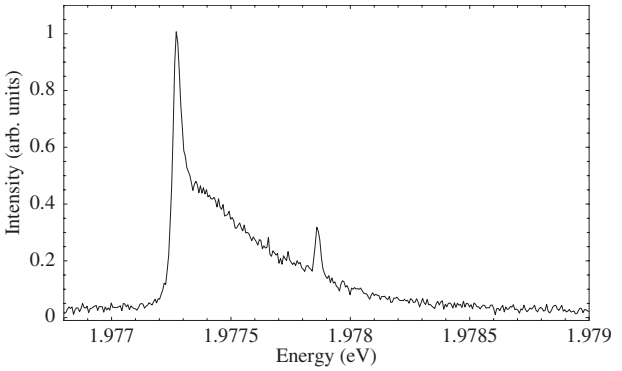

FIG. 6. Γ_2^- phonon-assisted luminescence of paraexciton for resonant excitation of paraexciton at 10 T and 1.3 K.

Besides the Γ_3^- and Γ_5^- phonon replica, we were able to measure the Γ_2^- (Fig. 6) and the Γ_4^- (Fig. 7) phonon emission. The narrow line at 1.97 786 eV (Fig. 6) is probably due to a bound exciton emission. From our data we get $E(\Gamma_2^-)=43.3$ meV, which agrees well with Ref. 15. The Γ_4^- phonon has to be considered as a polariton, since it is dipole allowed. Thus we expect a single longitudinal $[E(\Gamma_{4,\mathrm{LO}}^-)=19.1$ meV] and doubly degenerate transversal components $[E(\Gamma_{4,\mathrm{TO}}^-)=18.8$ meV]. The splitting of 0.3 meV is confirmed.[15]

With our method of resonant excitation of paraexcitons, we are even able to detect two-phonon processes. In Fig. 8 we present two-phonon sidebands of the paraexciton at 10 T. From the energy shifts of 24.2 and 27.2 meV, we assign these resonances to $(\Gamma_3^-+\Gamma_5^-)$ and $2\Gamma_3^-$ processes, respectively. Although a two-phonon Raman process is forbidden due to parity, one observes a luminescence signal. The scattering becomes allowed with increasing k since the distance to the zone center increases and parity is no longer conserved. As scattering at high k values is favored as compared to scattering at $k=k_0$, one does not observe a Raman resonance. The two phonon lines can be distinguished from excitons bound to impurities by variation of the excitation intensity. For high excitation intensity $I=3$ kW/cm^2, impurity lines are saturated (solid line in Fig. 8), whereas for low excitation

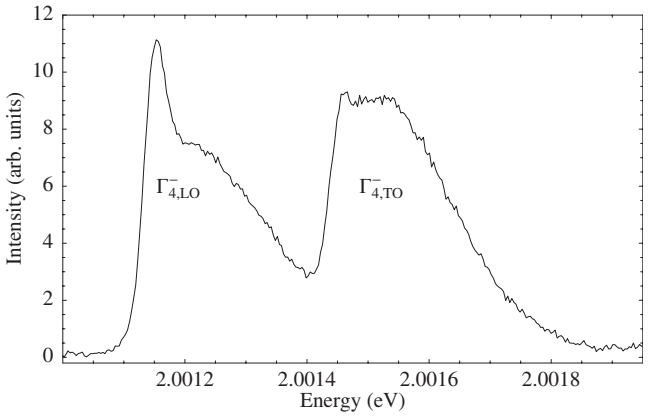

FIG. 7. Γ_4^- phonon-assisted luminescence of paraexciton for resonant excitation of paraexciton at 10 T and 1.3 K.

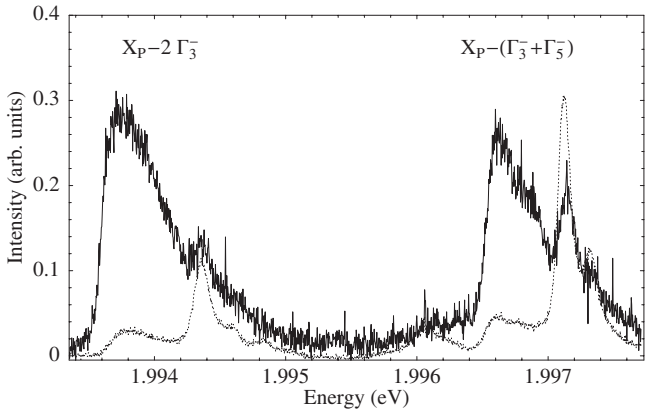

FIG. 8. Two-phonon-assisted paraexciton luminescence at 10 T and 1.2 K for two different excitation intensities: solid line, $I=3$ kW/cm^2; dotted line, $I=1$ W/cm^2.

intensity $I=1$ W/cm^2 (dotted line in Fig. 8) the phonon replicas are much weaker as compared to the impurity lines.

V. CONCLUSIONS

We have shown that with excitation in the orthoexciton, the ratio of the integrated intensity of the paraexciton Γ_3^- and Γ_5^- phonon replica depends quadratically on the magnetic field. By excitation in the orthoexciton or even at higher energy (phonon sideband of the orthoexciton or band to band transition), the thermal distribution of paraexcitons was observed in former experiments only via the emission of Γ_5^- phonons.[6,16] Resonant excitation yields in addition a Raman peak, which we clearly resolve for the Γ_2^-, Γ_3^-, Γ_4^-, and Γ_5^- optical phonons. As expected, the Γ_4^- phonon replica shows a splitting of 0.3 meV into a longitudinal and a transverse component. We observe a difference in width between the Γ_3^- ($\gamma_3=25$ μeV) and Γ_5^- ($\gamma_5=11$ μeV) resonance Raman peaks. For the narrow Γ_5^- emission ($\gamma_5=11$ μeV), our resolution of about 10 μeV should allow the detection of a population of paraexcitons at $k=0$ caused by BEC.

ACKNOWLEDGMENTS

We acknowledge the support by the Deutsche Forschungsgemeinschaft (SFB "Starke Korrelationen im Strahlungsfeld", Graduiertenkolleg "Materialeigenschaften und Konzepte für die Quanteninformationsverarbeitung", and Forschergruppe "Quantenoptik in Halbleitern").

*christian.sandfort@e2.physik.uni-dortmund.de

[1] A. Z. Genack, H. Z. Cummins, M. A. Washington, and A. Compaan, Phys. Rev. B **12**, 2478 (1975).
[2] P. Y. Yu and Y. R. Shen, Phys. Rev. B **12**, 1377 (1975).
[3] G. Baldassarri Höger von Högersthal, D. Fröhlich, M. Kulka, T. Auer, M. Bayer, and H. Stolz, Phys. Rev. B **73**, 035202 (2006).
[4] J. Wolfe, J. Lin, and D. W. Snoke, *Bose Einstein Condensation* (Cambridge University Press, Cambridge, 1995), Chap. 13, p. 281.
[5] N. Naka and N. Nagasawa, Phys. Rev. B **65**, 075209 (2002).
[6] A. Mysyrowicz, D. Hulin, and A. Antonetti, Phys. Rev. Lett. **43**, 1123 (1979).
[7] J. I. Jang, K. E. O'Hara, and J. P. Wolfe, Phys. Rev. B **70**, 195205 (2004).
[8] D. Hulin, A. Mysyrowicz, and C. Benoità la Guillaume, Phys. Rev. Lett. **45**, 1970 (1980).
[9] D. Fröhlich, G. Dasbach, G. Baldassarri Höger von Högersthal, M. Bayer, R. Klieber, D. Suter, and H. Stolz, Solid State Commun. **134**, 139 (2005).
[10] G. Kuwabara, M. Tanaka, and H. Fukutani, Solid State Commun. **21**, 599 (1977).
[11] J. Brandt, D. Fröhlich, C. Sandfort, M. Bayer, H. Stolz, and N. Naka, Phys. Rev. Lett. **99**, 217403 (2007).
[12] D. Fröhlich, J. Brandt, C. Sandfort, M. Bayer, and H. Stolz, Phys. Status Solidi B **243**, 2367 (2006).
[13] G. Dasbach, D. Fröhlich, H. Stolz, R. Klieber, D. Suter, and M. Bayer, Phys. Rev. Lett. **91**, 107401 (2003); G. Dasbach, D. Fröhlich, R. Klieber, D. Suter, M. Bayer, and H. Stolz, Phys. Rev. B **70**, 045206 (2004).
[14] G. F. Koster, J. O. Dimmock, R. G. Wheeler, and H. Statz, *Properties of the Thirty-Two Point Groups* (MIT, Cambridge, MA, 1963).
[15] K. Reimann and K. Syassen, Phys. Rev. B **39**, 11113 (1989).
[16] D. P. Trauernicht, J. P. Wolfe, and A. Mysyrowicz, Phys. Rev. B **34**, 2561 (1986).